Clim Dyn (2012) 39:1373–1383
DOI 10.1007/s00382-011-1129-7

Recent and future sea surface temperature trends in tropical pacific warm pool and cold tongue regions

Soon-Il An · Ji-Won Kim · Seul-Hee Im · Beak-Min Kim · Jae-Heung Park

Received: 16 May 2011 / Accepted: 17 June 2011 / Published online: 28 June 2011
© Springer-Verlag 2011

Abstract Using coral data, sea surface temperature (SST) reanalysis data, and Climate Model Intercomparison Project III (CMIP3) data, we analyze 20th-century and future warm pool and cold tongue SST trends. For the last 100 years, a broad La Nina-like SST trend, in which the warming trend of the warm pool SST is greater than that of the cold tongue SST, has appeared in reanalysis SST data sets, 20C scenario experiments of the CMIP3 data and less significantly in coral records. However, most Coupled General Circulation Models subjected to scenarios of future high greenhouse gas concentrations produce larger SST warming trends in cold tongues than in warm pools, resembling El Nino-like SST patterns. In other words, warmer tropical climate conditions correspond to stronger El Nino-like response. Heat budget analyses further verify that warmer tropical climates diminish the role of the ocean's dynamic thermostat, which currently regulates cold tongue temperatures. Therefore, the thermodynamic thermostat, whose efficiency depends on the mean temperature, becomes the main regulator (particularly via evaporative cooling) of both warm pool and cold tongue temperatures in future warm climate conditions. Thus, the warming tendency of the cold tongue SST may lead that of the warm pool SST in near future.

S.-I. An (✉) · S.-H. Im · J.-H. Park
Department of Atmospheric Sciences, Yonsei University, Seoul 120-742, Korea
e-mail: sian@yonsei.ac.kr

J.-W. Kim
APEC Climate Center, Pusan, Korea

B.-M. Kim
Korea Polar Research Institute, KORDI, Incheon, Korea

1 Introduction

The equatorial western Pacific, referred to as the 'warm pool', routinely records the warmest sea surface temperatures (SSTs) in the world. The equatorial eastern Pacific, or so-called 'cold tongue', is always a few degrees colder than the warm pool SST, even though it is at the same latitude, because of strong adiabatic cooling by equatorial upwelling. The thermal contrast between the two regions generates zonal overturning atmospheric circulation (Lindzen and Nigam 1987), or 'Walker circulation' (Walker 1924; Bjerknes 1969), which in turn, causes further cooling of the cold tongue through equatorial upwelling. This feedback process is referred to as 'Bjerkness feedback' (Bjerknes 1966, 1969). Moreover, the warming of the warm pool due to increasing concentrations of greenhouse gases has been greater than that of the cold tongue during the last 100 years (Sun and Liu 1996; Cane et al. 1997; Seager and Murtugudde 1997; Karnauskas et al. 2009), which has prompted a stronger Walker circulation, sometimes called a 'La Nina-like' response. Note that some recent studies, such as DiNezio et al. (2009a, b), have suggested that 'El Nino-like' or 'La Nina-like' are not appropriate expressions. However, we will use those expressions here because the zonal contrast of SST anomaly during each event still resembles that of SST trends. The rising concentration of greenhouse gases in the atmosphere has resulted in increased backward longwave radiation, thereby causing SSTs in both the warm pool and cold tongue regions to rise. The warming trend in the warm pool region, with its deep-ocean mixed layer, is weaker than the trend in the cold tongue, with its shallow mixed layer. Yet, mixed layer cooling by the upwelling in the cold tongue region overcompensates for the surface radiative warming (i.e., the ocean dynamical thermostat; Clement et al. 1996).

Moreover, the subsurface warming occurs over a time frame of a few decades (An et al. 2008), so the previous surface warming results in a strong vertical ocean temperature gradient in the cold tongue region, which promotes surface cooling by vertical transport of cold water. Consequently, greenhouse warming initially causes a stronger warming trend over the warm pool region than in the cold tongue region. Even so, as the subsurface temperatures increase, the vertical temperature gradient decreases and the surface cooling due to upwelling weakens. Hence, the net thermal damping can decline, as shown in Xie et al. (2010), causing the warming of the cold tongue possibly to exceed that of the warm pool.

The tropical Pacific interacts more strongly with the atmosphere than any other area in any other ocean. Therefore, when Walker circulation becomes weaker or stronger, it triggers positive feedback, i.e., 'Bjerkness feedback', such that the weaker the upwelling, the warmer the cold tongue, and vice versa. (The general reduction of circulation is often reported as a possible consequence of increased dry static stability in warmer climates; Knutson and Manabe 1995; Sugi et al. 2002.) In this regard, once the warming trend of the cold tongue overtakes the warming trend of warm pool, then the latter cannot subsequently surpass the former. However, it is still unclear whether the weakening of Walker circulation (Held and Soden 2006; Vecchi et al. 2006; Vecchi and Soden 2007) is a cause or an effect of the subsurface warming; although, definitively determining this order may be difficult because of their tight interaction.

In this study, we compute SST trends over the warm pool and cold tongue for approximately the last 100 years using various data. We also compute the future trends of each region using Climate Model Intercomparison Project III (CMIP3) data, particularly utilizing the experimental results for the CO_2 doubling and quadrupling scenarios from the Intergovernmental Panel on the Climate Change Fourth Assessment Report (IPCC AR4). Furthermore, we analyze the surface energy budget over the warm pool and cold tongue to quantify how much the radiative forcing and the dynamical cooling change in different scenarios. Section 2 introduces the relevant data. Section 3 addresses changes in SST trends over the warm pool and cold tongue regions as well as surface energy budgets. Concluding remarks are presented in Sect. 4.

2 Data

Three types of data are analyzed in this study. The following subsections document each data set.

2.1 Proxy data from coral records

Modern coral records for the tropical Pacific were obtained from the NOAA National Climate Data Center (http://www.ncdc.noaa.gov/paleo/indexcoral.html). Each data set covers different periods, so for ease of comparison, all of the calculations were performed on data from 1930 to the present. The trend was then computed using the least-squares method. The locations and other information for each data set are listed in Table 1.

2.2 Analysis data

Two sets of monthly-mean SST analysis data were utilized. One was obtained from the Extended Reconstruction Sea Surface Temperature Version 3 (ERSSTv3; Reynolds et al. 2007), which spans from January 1854 to December 2009. The other was obtained from the UK Met Office Hadley Centre's Global Sea-Ice and SST data version 1 (hereafter, HadISST1; Rayner et al. 2003), which spans from January

Table 1 Linear trend of $\delta^{18}O$ obtained from coral data in ‰ per decade year

Name	Location	Period	$\delta^{18}O$	Reference
Lombok Strait, Bunaken Island	1.5 N-8.5 S, 115.5-124.83 E	1930–1990	−0.015*	Charles et al. (2003)
Madang Lagoon	5.22 S, 145.82 E	1930–1991	−0.023*	Tudhope et al. (1995)
Rabaul	4.18 S, 151.98 E	1930–1997	0.002*	Quinn et al. (2006)
Nauru Island	0.5 S, 166 E	1930–1995	−0.079*	Guilderson et al. (1998)
Maiana	1 N, 173 E	1930–1994	−0.079*	Urban et al. (2000)
Palmyra Island	5.87 N, 162.13 W	1930–1998	−0.056*	Cobb et al. (2001)
Kiritimati Island	2 N, 157.3 W	1938–1993	−0.026*	Evans et al. (1998)
Clipperton Atoll	10.3 N, 109.22 W	1930–1994	−0.015*	Linsley et al. (2000)
Punta Pitt	0.67 N, 89.17 W	1936–1982	−0.008*	Shen et al. (1992)
Secas Island	7.95 N, 82 W	1930–1984	−0.021*	Linsley et al. (1994)

* The results that pass the significance test at a 95% confidence level

Table 2 CMIP3 model configurations

No.	Model	Institution	Atmospheric resolution	Ocean resolution
1	CCSM3	NCAR (USA)	T85L26	1.125° × 0.27°L40
2	ECHAM5/MPI-OM	MPI-M (Germany)	T63L31	1.5° × 0.5°L40
3	GFDL-CM2.0	GFDL (USA)	2.5° × 2°L24	1° × 0.33°L50
4	GFDL-CM2.1	GFDL (USA)	2.5° × 2°L24	1° × 0.33°L50
5	GISS-ER	NASA/GISS (USA)	5° × 4°L20	5° × 4°L13
6	INGV-ECHAM4	INGV (Italy)	T106	1.125° × 1.125°
7	INM-CM3	INM (Russia)	5° × 4°L21	2.5° × 2°L33
8	IPSL-CM4	IPSL (France)	2.5° × 3.75°L19	2° × 0.5°L31
9	MIROC3.2(medres)	CCSR/NIES/FRCGC (Japan)	T42L20	1.4° × 0.5°L43
10	MIUB-ECHOG	MIUB (Germany)	T30L19	T42L20
11	MRI-CGCM2.3.2	MRI (Japan)	T42L30	2.5° × 0.5°L23

1870 to June 2008. From these data sets, we calculated the warm pool and cold tongue SSTs, which were defined as the average SST over 120°–160°E, 5°S–5°N (hereafter, symbolically T_W) and 170°–120°W, 5°S–5°N (hereafter, symbolically T_E), respectively.

2.3 Coupled general circulation models

The multi-model experimental data from the World Climate Research Program Coupled Model Intercomparison Project 3 Program (WCRP CMIP3; https://esg.llnl.gov:8443/index.jsp) were used for calculations of the twentieth-century and future trends of the tropical Pacific SST. In this paper, we used the twentieth-century (20C3M), CO_2 doubling ($2CO_2$), and CO_2 quadrupling ($4CO_2$) scenario experiments. The twentieth-century experiments include data from 1850 to 2000 AD, which were simulated under various climate forcings such as greenhouse gases, insolation, volcanic forcing, and the aerosol effect. The CO_2 doubling and quadrupling experiments simulate the projected response to a 1% per year increase of CO_2 concentration. Both CO_2 experiments were started at 348 ppmv and then increased to 696 ppmv for the doubling experiment and 1,392 ppmv for the quadrupling experiment, and were integrated continuously with the fixed CO_2 concentration rate. A simple description of the 11 models used in this study can be found in Table 2.

3 Results

3.1 Trends in coral data

Long-term observations over the tropical Pacific spanning more than a century are rare. Therefore, proxy data, like coral data, are frequently used to investigate the features of long-term tropical climate variability. Here, we analyze the available coral data (Table 1), particularly data observed near the equatorial Pacific region, which extends from the maritime continents in the tropical western Pacific to the eastern coast of the tropical Pacific. Since $\delta^{18}O$ is frequently used as a proxy for temperature, we computed the linear trend of $\delta^{18}O$ obtained from each coral data set (Fig. 1). Negative linear trends, indicating warming trends (e.g., Bradley 1999), were observed from all coral records, except for samples from Rabaul, which is adjacent to the southwest coast of New Zealand. The linear trends over the western-to-central Pacific (Nauru Island, Maiana, Palmyra Island) are larger and then slightly decrease in the eastern Pacific (Kiritimati Island and Clipperton Atoll). Samples from near the west coast of the American continent (Punta Pitt and Secas Island) and those from the coast of the maritime continent (Bunaken Island, Madang Lagoon) show a similar linear trend. In summary, the linear trends obtained from the coral data show the strong warming trend over the far western to central Pacific and the

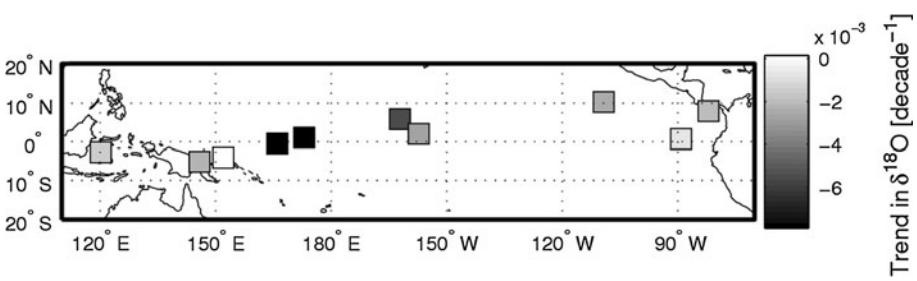

Fig. 1 Linear trend of $\delta^{18}O$ obtained from coral data. All values are statistically significant with 95% confidence. The negative values correspond to warming trends

relatively weak warming trend over the eastern Pacific. However, more samples of coral data are necessary to lead to a significant conclusion.

3.2 Recent SST trends from reanalyses of SST and CMIP3 data

To depict the recent tropical SST trends, the linear trends were computed using the two different reanalysis SST data sets. For preprocessing, the annual mean values were computed and then the 10-year moving average was taken in order to remove interannual-to-decadal variation. The least-squares method was then used to compute trends. As seen in Fig. 2, the linear trend for the last 100 years in the tropical Pacific indicates overall warming. In both data sets (ERSSTv3 and HadISST1), the trend in the warm pool SST is slightly greater than that in the cold tongue SST, meaning that the same intensified zonal contrast of the equatorial Pacific SST was observed as seen in other studies (Clement et al. 1996; Sun and Liu 1996; Cane et al. 1997; Seager and Murtugudde 1997; Karnauskas et al. 2009). However, the two data sets show different features, especially over the cold tongue region, where ERSSTv3 presents a warming trend while HadISST1 shows a cooling trend. In addition, a cautionary note on the reanalysis SST data was recently raised by Deser et al. (2010). They analyzed the non-interpolated HadISST1 data and found no visible cooling trend of the SST over the cold tongue region. They further stressed the uncertainty in the current reanalysis data, suggesting that insufficient observations over areas such as the cold tongue could result in underloaded interpolations. Consequently, it is evident that the SST trends derived from recent data exhibit uncertainty; however, we confirm consistent results between the reanalyzed SST data, particularly from ERSSTv3 and the coral data in terms of the zonal contrast of the linear trend, such as strong warming trends over the western-to-central Pacific and west coast and weak warming trends over the eastern Pacific.

Before the Tropical Atmosphere Ocean Project (TAO; http://www.pmel.noaa.gov/tao/), observation in the tropical Pacific was very limited. This limitation is a factor underlying the uncertainty of SST trend estimates that is not easily overcome. Therefore, rather than computing the absolute SST trends of the warm pool and cold tongue regions in the present study, we computed the slope

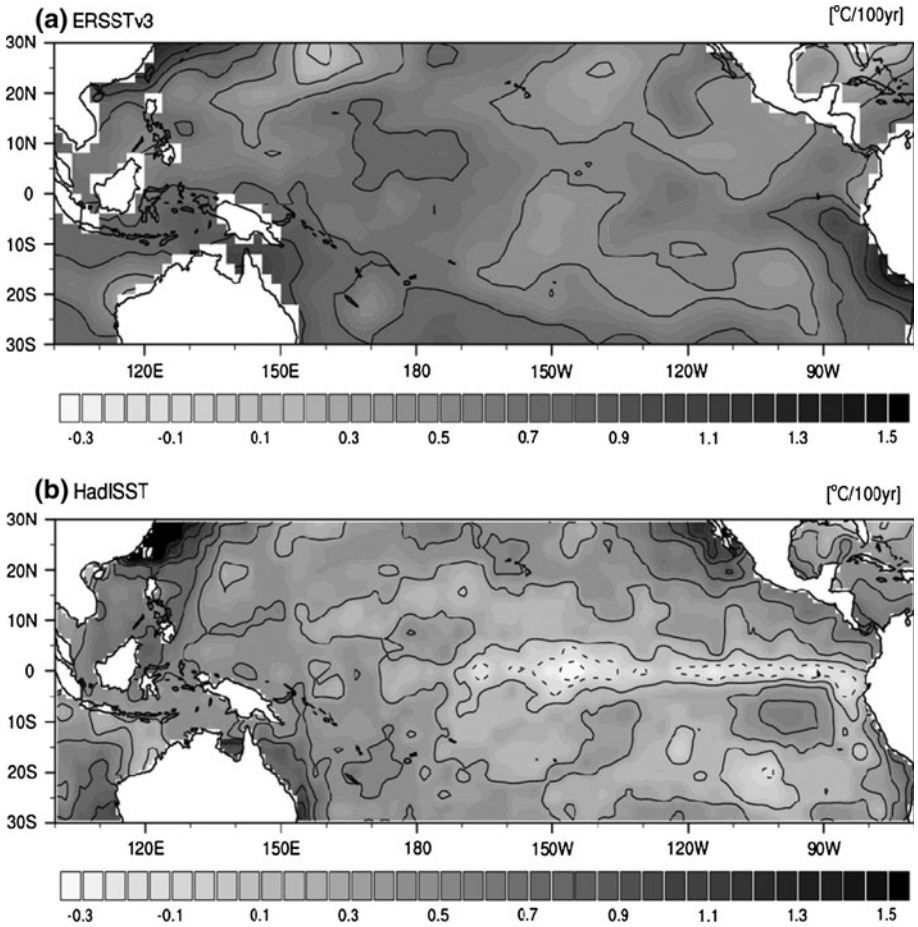

Fig. 2 SST trends over the tropical Pacific computed using **a** ERSSTv3 for the years 1900–2009 and **b** HadISST1 for the years 1900–2007. Contour intervals are 0.2°C/100 years. Negative values are indicated by *dashed line*

(indicated by coefficient, 'a') of the least-square line between the warm pool SST (T_W) and the cold tongue SST (T_E). As shown in the Appendix, the slope indicates the ratio between the warm pool SST trend and the cold tongue SST trend, which seems to provide more consistent results for both data sets than seen in Fig. 2. Together with the slope, we computed the coefficient of determination (denoted by R^2), which indicates what proportion of the variance in T_E is predictable by T_W. The dependency of T_E on T_W is first related to external forcing (i.e., possible backward longwave radiative forcing associated with increased concentrations of greenhouse gases) that underlies the same directional changes in both T_E and T_W. Second, it is related to the dynamical connection between T_E and T_W through air-sea coupling and zonal thermal advection. Thus, when longwave forcing from the greenhouse effect dominates change in the SST, R^2 should increase. Conversely, dominant nonlinear processes or longer-time-scale natural variation when changing the SST may reduce R^2. Hence, the value of the slope and R^2 represent the inherent physical properties of each data set and can be used as an alternative means of measuring SST trends.

Figure 3 shows scatter plots of T_E versus T_W obtained from ERSSTv3 and HadISST1 for the last 100 years. The slopes for both data sets are less than 1, indicating that the linear warming trend of T_W is greater than that of T_E; however, the exact values for the slope and R^2 are notably different—i.e., $a = 0.77$ and $R^2 = 0.40$ from the ERSSTv3 data and $a = 0.54$ and $R^2 = 0.21$ from the HadISST1 data. The relatively small a and R^2 from HadISST1 may be attributed to the independently occurring, strong, long-term fluctuations in each region but an in-depth investigation of this effect is outside the scope of this study. Note that the slope for HadISST1 does not pass the 95% statistically significant level test. Overall, for the last 100 years, the warming trend of the SST over the warm pool region (hereafter referred to as the 'La Nina-like response') has been larger than that over the cold tongue region (hereafter referred to as the 'El Nino-like response').

The relative linear trend between the warm pool and cold tongue was further analyzed using CMIP3 data. In particular, it was integrated in accordance with the guidelines for "20-century external forcing," (20C3M experiment). By comparing these results with previously observed results, we were able to examine the validity of the CMIP results as well as to establish guidelines by which to measure the extent that the tropical Pacific SST has responded to increasing greenhouse gas concentrations. Here, we used the output from 11 models, as listed in Table 2, and more than 100 years of data from each model for computation. As with the assimilation data, the relative trends between the warm pool and cold tongue SSTs were computed and plotted. From Fig. 4, we see that 8 out of the 11 models show results similar to the observations, namely the La Nina-like response. The exact values for the slope and R^2 are listed in Table 3. The slopes for most of the models are greater than those for the observations, except for the slope from MPI_echam5 ($a = 0.405$), which is not statistically significant. Strangely, the scatter of MPI_echam5 is confined within a short range of both T_W and T_E (less than 1 degree). Additionally, the SST in MPI_echam5 is strongly stabilized, possibly as a result of intense temperature regulating processes. On the other hand, most of the models, including IPSL_CM4, GFDL_CM2.0, MIROC3.2_medres, NCAR_CCSM3.0, MIROC3.2_hires, INM_CM3 and MRI_cgcm2.3.2a, possess large, statistically significant slopes with 95% confidence. In these models, changes in the warm pool and cold tongue SSTs are tightly correlated; however, it is difficult to determine whether this correlation reflects responses to the same external forcing or to the internal dynamical processes between the two regions. The SST of the warm pool is mainly regulated through the so-called thermodynamical thermostat (e.g., surface evaporative cooling and cloud radiative forcing; Sun and Liu 1996), while the cold tongue SST is regulated primarily through the ocean dynamical thermostat (e.g., upwelling of cold subsurface water; Clement et al. 1996). Thus far, since the observations and the Coupled general circulation models (CGCMs) show

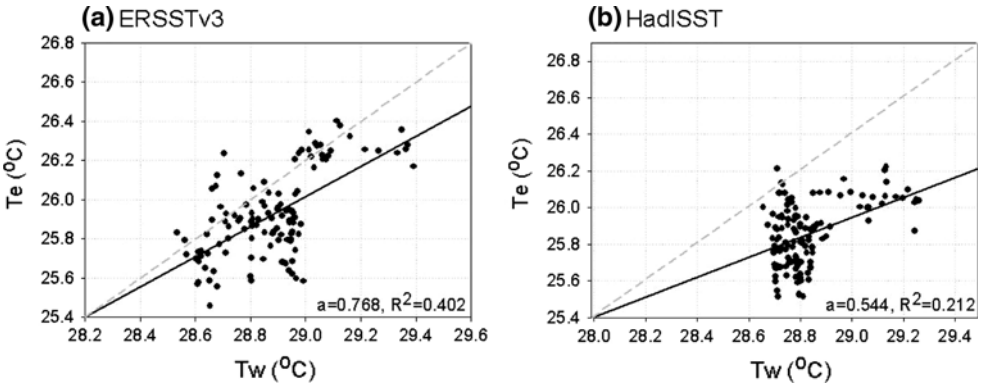

Fig. 3 *Scatter plot* of the warm pool temperature (T_W) versus the cold tongue temperature (T_E) using **a** ERSSTv3 and **b** HadISST1. The *dark solid line* indicates the least-square fitted curve between T_W and T_E. Slopes of each curve are given in the *lower right corner* of each diagram. *Dashed line* indicates a line for $a = 1$

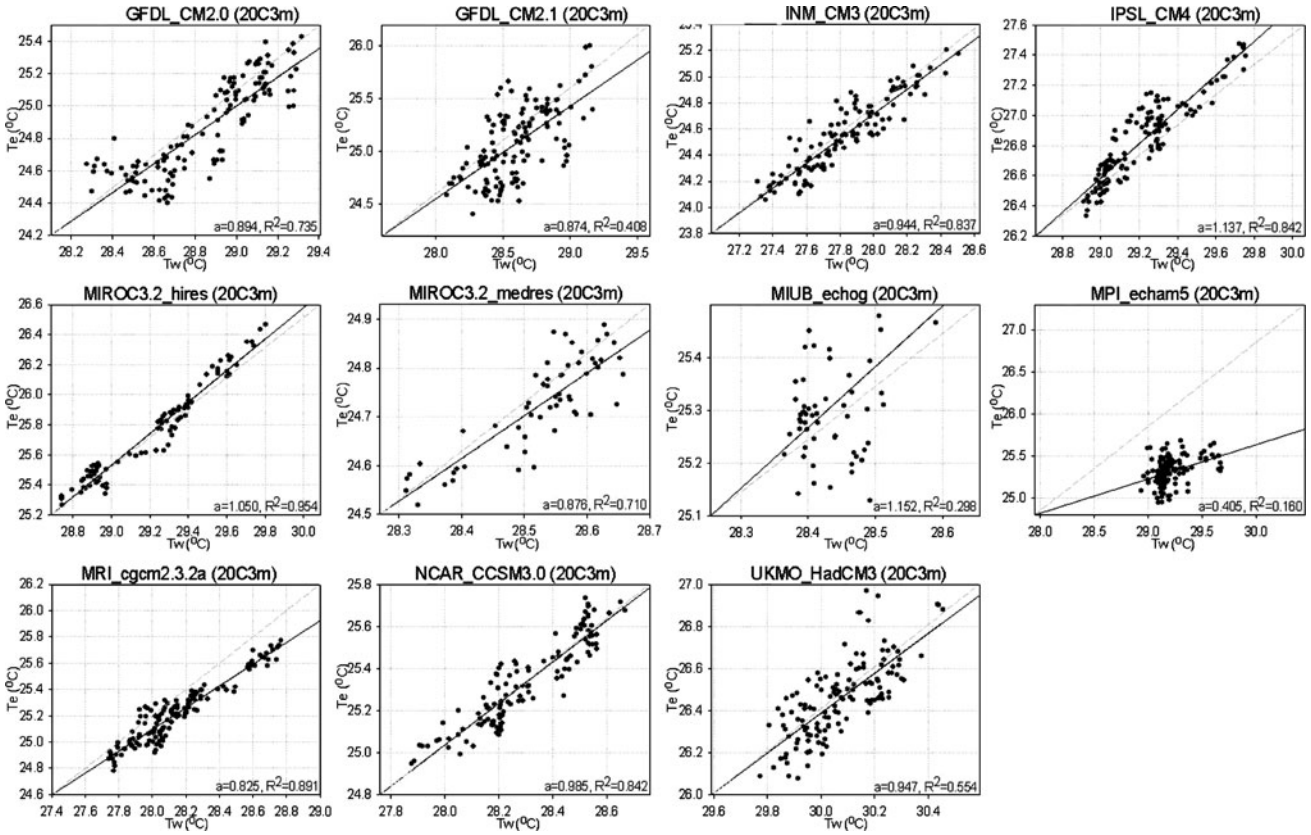

Fig. 4 *Scatter plots* like those for Fig. 3, except using the 20-century scenario experiments of the CGCMs

Table 3 Slope of the linear trend and its least-square error (in parentheses) obtained from each data set

	Twentieth century	$2CO_2$	$4CO_2$
ERSSTv3	0.768* (0.402)		
HadISST1	0.544 (0.212)		
INM_CM3	0.944* (0.837)	0.885* (0.951)	0.938* (0.986)
GFDL_CM2.0	0.894* (0.735)	1.160* (0.934)	1.166* (0.991)
GFDL_CM2.1	0.874* (0.408)	1.239* (0.827)	1.067* (0.978)
MIROC3.2_medres	0.876* (0.710)	1.176* (0.992)	1.224* (0.998)
MPI_echam5	0.405 (0.160)	1.249* (0.872)	1.190* (0.959)
MRI_cgcm2.3.2a	0.825* (0.891)	1.116* (0.959)	1.177* (0.992)
NCAR_CCSM3.0	0.985* (0.842)	1.050* (0.964)	1.225* (0.988)
UKMO_HadCM3	0.947* (0.554)	1.186* (0.968)	
MIUB_echog	1.152 (0.298)	1.170* (0.975)	1.221* (0.996)
MIROC3.2_hires	1.050* (0.954)	1.219* (0.998)	
IPSL_CM4	1.137* (0.842)	1.046* (0.983)	

* The results that pass the significance test at a 95% confidence level. Units are dimensionless

mostly La Nina-like responses, it can be suggested that the ocean dynamical thermostat more strongly regulates the cold tongue SST than the thermodynamical thermostat does the warm pool SST. Furthermore, in the tropical Pacific, the warm pool and cold tongue SSTs are tightly linked through Bjerkness feedback (Bjerkness 1969), which is the most dominant air-sea coupling process in the entirety of the global ocean. Since Bjerkness feedback is strongly associated with air-sea interaction, the tendency of the cold tongue SST will be opposite the tendency of the warm pool SST because of the intense ocean dynamical thermostat, like that which occurs during a La Nina event. Therefore, the relatively weak warming tendency of the cold tongue SST than the warm pool SST during the 20th century is presumably due to the compensation by the ocean dynamical cooling (e.g., Clement et al. 1996; DiNezio et al. 2009b). Nevertheless, in the following section, we will show that the role of the ocean dynamical

thermostat decreases while the role of the thermodynamical thermostat increases as the globe climate warms.

3.3 Future SST trends

In this section, we compute the relative linear trend between the warm pool and cold tongue SSTs using the CO_2 doubling and quadrupling scenarios (the '$2CO_2$' and '$4CO_2$' experiments, respectively) experiments discussed in the previous sub-section. In the $2CO_2$ experiments, as seen in Fig. 5, ten out of 11 models showed an El Nino-like response. Seven models that initially showed a La Nina-like response in the 20C3M experiment actually changed to El Nino-like responses. Similar results were observed for the $4CO_2$ experiments, as shown in Fig. 6. Seven out of eight models showed an El Nino-like response. In fact, INM_CM3 was the only model to show a La Nina-like response in both the $2CO_2$ and $4CO_2$ experiments. Furthermore, as the greenhouse gas concentrations increased (i.e., from 20C3M levels to $2CO_2$ levels and then further to $4CO_2$ levels), both the slope and R^2 increased, implying that the tendencies of both the warm pool and cold tongue SSTs are strongly affected by greenhouse gas concentrations. It is likely that the ocean dynamical thermostat becomes weaker with higher greenhouse gas concentrations so that the warming tendency of the cold tongue SST becomes larger than that of the warm pool SST. This point will be confirmed in the next subsection.

The tropical Pacific basin-wide warming tendency observed in the proxy data, reanalysis observation data, and various CGCM data reflects the dominant effect of increasing greenhouse gas concentrations on global warming. However, local feedback processes modify the actual regional responses, creating either El Nino- or La Nina-like patterns. In Fig. 7, we present the scatter diagram of the areal-mean SSTs (warm pool SST and cold tongue SST) and the slopes that were shown in previous sections. A systematic transition from the La Nina-like response to the El Nino-like response as the mean SST increases is clearly observed. This transition implies that warmer tropical climate conditions (which are also associated with higher greenhouse gas concentrations) may induce regime transition from a La Nina-like response to an El Nino-like response, thereby potentially degrading the effect of the ocean dynamical thermostat.

3.4 Possible interpretations

Analysis of the CGCM data provides a clue as to why the La Nina-like response to mild tropical warming becomes

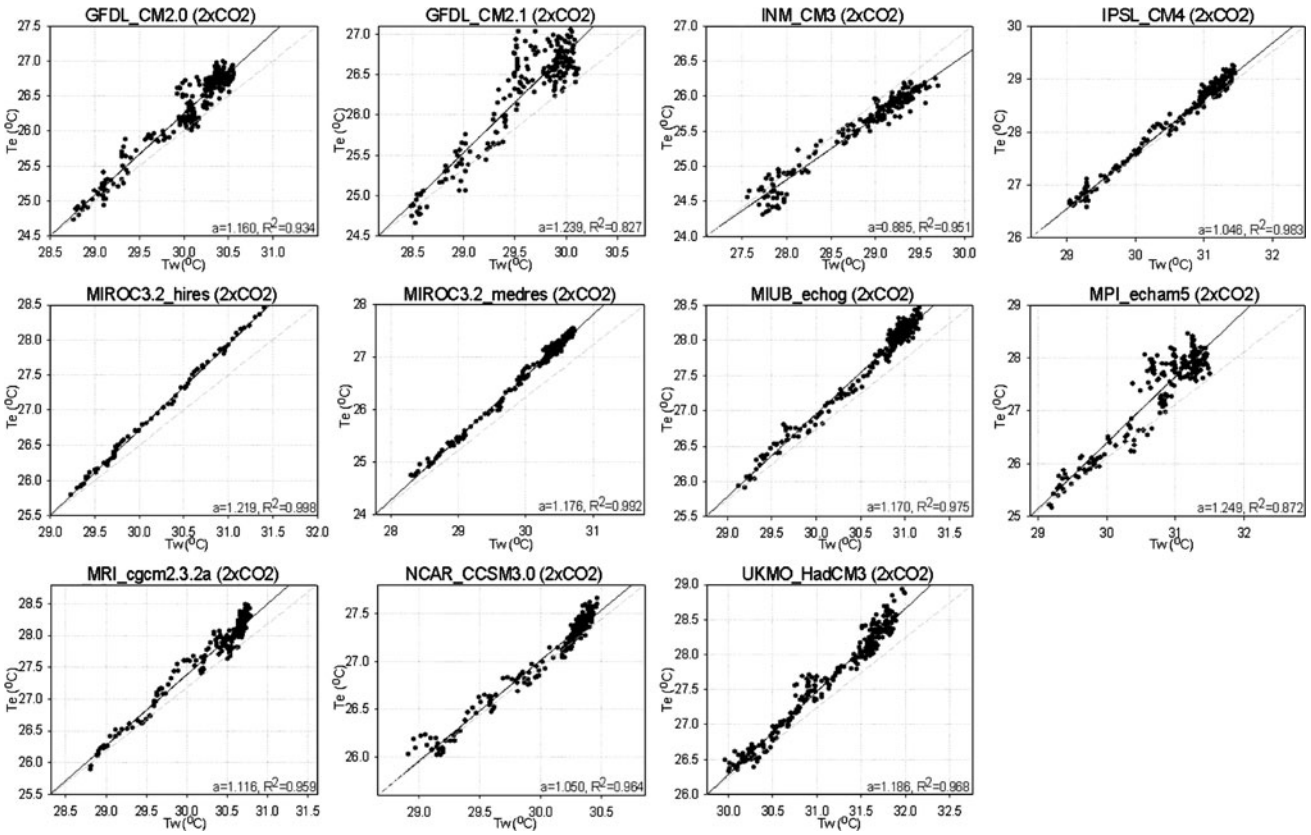

Fig. 5 *Scatter plots* like those for Fig. 4 except using the data from the CO_2 doubling scenario experiments

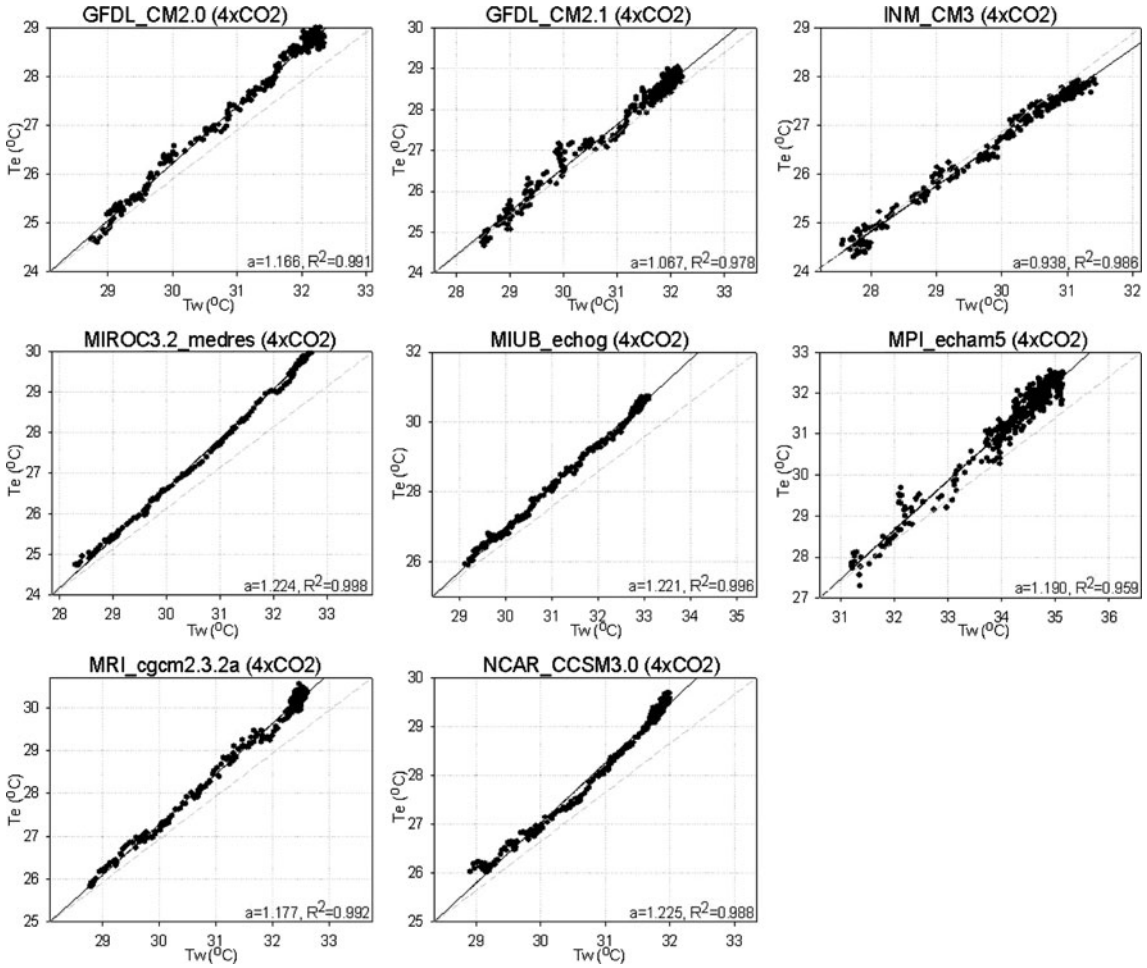

Fig. 6 *Scatter plots* like those for Fig. 4 except using the data from the CO_2 quadrupling scenario experiments

an El Nino-like response to severe tropical warming: it must be related to a change in the efficiency of the temperature-regulating "thermostat." To assess the efficiency of the thermostat quantitatively, we performed a heat budget analysis of the cold tongue region (which is the same as the Nino3.4 region bounded by 5°N–5°S, from 170°W to 120°W). Using the CMIP data, we computed the average annual downward radiative heat flux and vertical thermal advection in the ocean mixed layer over the cold tongue region. We then computed the linear regression coefficients between these two processes in order to quantify the dynamical relationship between the warming by the surface heat flux and the cooling by the upwelling, an effect of the ocean dynamical thermostat. The surface radiative heat flux here includes the downward long-wave and short-wave radiation, and the vertical advection implies $-\frac{\bar{W}(d\bar{T})}{dZ}$, where the upper bar indicates the annual mean. Both are in units of W/m^2. The vertical advection defined here always exerts a cooling effect; thus, the radiative surface heating in the cold tongue region is partly suppressed by vertical thermal advection in order to maintain the heat balance, keeping the cold tongue temperatures colder. As listed in Table 4, the surface radiative heating and the vertical advective cooling are positively correlated in all models, indicating that higher surface heating is associated with weaker vertical advective cooling. Interestingly, the cooling rate due to vertical advection with respect to surface heating decreases as greenhouse gas concentrations increase, although the slopes are not statistically significant in some of the models. Additionally, analysis of the relationship between surface radiative heating and surface evaporative cooling (i.e., latent heat release) shows that they are positively correlated in all models, as seen in Table 5. This positive correlation indicates that higher surface warming is associated with stronger evaporative cooling. These results are much more significant than those of the cases for the upwelling cooling. In short, as greenhouse gas concentrations increase, the cooling effect by the latent heat flux increases but the cooling effect by the upwelling actually decreases. The higher climatological SST in the warm pool region generates stronger evaporative cooling than the lower

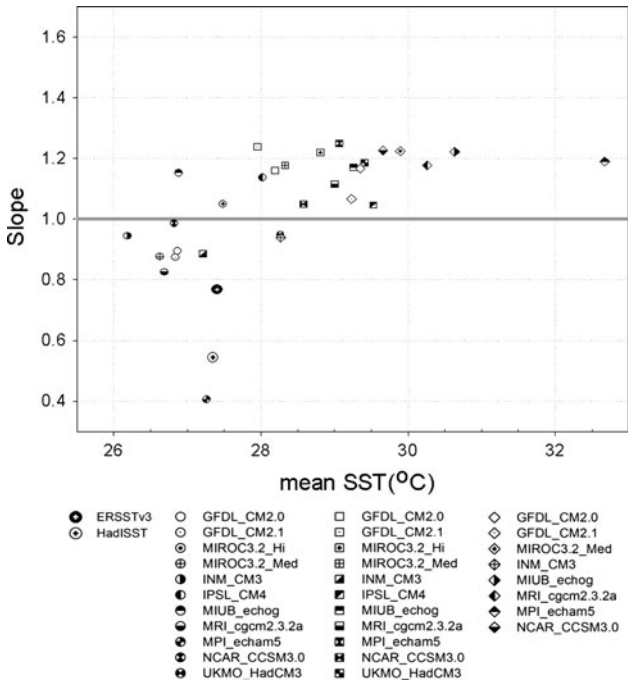

Fig. 7 *Scatter plot* showing the mean SST for the indicated models and the slope of the least-squares trend. *Circle*, *rectangle*, and *diamond marks* indicate 20C scenario experiment, CO_2 doubling experiment, and CO_2 quadrupling experiment, respectively

climatological SST in the cold tongue region, particularly with respect to an anomalous change in the SST. Consequently, the effect of the thermodynamical thermostat in the cold tongue region is usually weaker than that in the warm pool region (Xie et al. 2010). Therefore, as shown in the CMIP results, if the ocean dynamical thermostat is either weakened or turned off as global warming progresses, an El Nino-like response of the tropical Pacific to the uniform surface warming would be expected. Xie et al. (2010) showed that global warming would nearly nullify the net effect of the oceanic thermal transport in the equatorial eastern Pacific because of the cancellation between the upwelling damping (i.e., the cooling by the vertical thermal advection) and the thermocline feedback. These effects are a result of the equatorial westerly anomalies associated with the decline of Walker circulation due to global warming (Vecchi et al. 2006), which not only weakens the upwelling damping but also acts to warm the water by deepening the thermocline, so-called 'thermocline feedback' (Vecchi and Soden 2007). Note that the sum of the upwelling damping and thermocline feedback in Xie et al. (2010) is identical to the cooling effect by the upwelling in this study. However, as shown in this study, even under a fixed greenhouse gas concentration, the cooling effect by the upwelling is reduced as the surface temperature increases. Therefore, the weakening of the ocean dynamical thermostat under warmer climate conditions is a natural process.

Table 4 Slope of the linear fit between the radiative heat flux and the vertical thermal advection

	Twentieth century	$2CO_2$	$4CO_2$
GFDL_CM2.0	0.0995*	0.2055**	0.2115*
GFDL_CM2.1	0.0008	0.1881**	0.2026*
MIROC3.2_medres	0.0652	0.0042	0.0793
MPI_echam5	0.0066	0.2219**	
MRI_cgcm2.3.2a	0.1049	0.2848*	0.0704
IPSL_CM4	0.1168	0.0947	

*, ** The results that pass the two-tails significance test at 90% and 95% confidence levels, respectively. Units are dimensionless

4 Concluding remarks

By analyzing coral proxy data, ocean reanalysis data, and CMIP3 data, we identified the strong possibility that a regime change from a 'La Nina-like' response to an 'El Nino-like' response to global warming will occur as a long-term trend. The coral proxy data provided a result consistent with that of the ocean reanalysis data at least for the open ocean, but the linear trend pattern of the observed tropical Pacific SST for the last 100 years is still unclearly defined (Deser et al. 2010). Nevertheless, the results from CMIP3 data were enough to conclude that the 'La Nina-like' pattern will change to an 'El Nino-like' pattern as global warming progresses. In particular, the cooling effect from evaporative cooling will increase as global warming intensifies, while that from vertical thermal advection will decrease. In other words, the ocean dynamical thermostat will "malfunction" slightly in warmer climate conditions.

Furthermore, we found that evaporative cooling acts to reduce surface warming without a time delay, while vertical thermal cooling does so with about a 1- to 11-month time lag. The relationship between evaporative cooling and the vertical advective cooling lag was confirmed by calculating the lag-correlation between the surface warming and the latent heating or vertical advective cooling (not shown here). This lag-correlation indicates that the evaporative cooling first neutralizes the radiative warming, and then, a few months later, prompts the vertical advective cooling to operate. The timing of vertical advective cooling is very important. Under the current climate conditions, the evaporative cooling over the cold tongue region may not be enough to fully compensate for the radiative warming. In other words, the delayed vertical advective cooling driven by the initial atmospheric response, which is a fast surface thermodynamical adjustment, may overcompensate for warming through slow adjustment so that the cold tongue temperature is lower than the warm pool temperature. However, as the climate becomes warmer, the evaporate cooling becomes enough to negate the surface warming (e.g., Xie et al. 2010).

Table 5 As in Table 4, except for the latent heat flux

	Twentieth century	$2CO_2$	$4CO_2$
GFDL_CM2.0	0.469**	0.532**	0.350
GFDL_CM2.1	0.476**	0.500*	0.421
MIROC3.2_medres	−0.016	0.741**	0.609*
MPI_echam5	0.905**	0.618**	
MRI_cgcm2.3.2a	0.530**	0.089	−0.692
IPSL_CM4	0.263**	0.376*	

A possible explanation for the malfunction of the ocean dynamical thermostat under conditions of global warming may be related to the delayed response of the oceanic subsurface temperature to global warming (An et al. 2008). In the initial stages of global warming, the delayed warming of the oceanic subsurface compared to the surface warming leads to a strong vertical stratification, which results in an intense cooling effect by the upwelling. However, as global warming progresses, the subsurface also becomes warmer, and together with the weakening of the surface warming due to the marked evaporative cooling in the higher SST regions, it results in the weakening of the cooling effect caused by the upwelling. Further analyses to test this hypothesis will be performed in a future study.

Acknowledgments The authors thank A. Timmermann for valuable discussion. This work was supported by the National Research Foundation of Korea (NRF) grant funded by the Korea government (MEST) (No. 2011-0015208). BM Kim was supported by Korea Meteorological Administration Research and Development Program under Grant RACS_2011-2019 (PN11020).

Appendix: Meaning of the slope in this study

Approximating the linear trends of variables X and Y using the method of least-squares gives the equations

$$X = a't + b' \quad (1)$$

$$Y = a''t + b'' \quad (2)$$

Then, the equation for the least-squares line between X and Y becomes

$$Y = aX + b, \quad (3)$$

where the constants a (slope) and b (intercept) can be found using the following equations:

$$a = \frac{N\sum XY - (\sum X)(\sum Y)}{N\sum X^2 - (\sum X)^2} \quad (4)$$

$$b = \frac{(\sum Y)(\sum X^2) - (\sum X)(\sum XY)}{N\sum X^2 - (\sum X)^2} \quad (5)$$

where N is the number of data. After substituting (1) and (2) into (4) and (5), we have $a = a''/a'$ and $b = b'' - b'(a''/a')$ so that a in Eq. (3) is the ratio between the trend of Y and that of X. Therefore, if a is greater than one, then the linear trend of Y is greater than that of X, and vice versa. However, this condition is only valid when a' and a'' are the same sign, and otherwise a has a negative value indicating that a' and a'' have opposite linear trends.

References

An S-I, Kug J-S, Ham Y-G, Kang I-S (2008) Successive modulation of ENSO to the future greenhouse warming. J Clim 21:3–21

Bjerknes J (1966) A possible response of the atmospheric Hadley circulation to equatorial anomalies of ocean temperature. Tellus 18:820–829

Bjerknes J (1969) Atmospheric teleconnections from the equatorial Pacific. Mon Weather Rev 97:163–172

Bradley RS (1999) Paleoclimatology: reconstructing climates of the quaternary, 2nd edn. Harcourt Academic Press, London

Cane MA, Clement AC, Kaplan A, Kushnir Y, Pozdnyakov D, Seager R, Zebiak SE, Murtugudde R (1997) Twentieth-century sea surface temperature trends. Science 275:957–960

Charles CD, Cobb K, Moore MD, Fairbanks RG (2003) Monsoon-tropical ocean interaction in a network of coral records spanning the 20th century. Mar Geol 201:207–222

Clement AC, Seager R, Cane MA, Zebiak SE (1996) An ocean dynamical thermostat. J Clim 9:2190–2196

Cobb KM, Charles CD, Hunter DE (2001) A central tropical Pacific coral demonstrates Pacific, Indian, and Atlantic decadal climate connections. Geophys Res Lett 28:2209–2212

Deser C, Phillips AS, Alexander MA (2010) Twentieth century tropical sea surface temperature trends revisited. Geophys Res Lett 37:L10701. doi:10.1029/2010GL043321

DiNezio PN, Clement AC, Vecchi GA (2009a) Is El Nino an appropriate analogue for tropical Pacific climate change? EOS 91:141–142

DiNezio PN, Clement AC, Vecchi GA, Soden BJ, Kirtman BP, Lee S-K (2009b) Climate response of the equatorial pacific to global warming. J Clim 22:4873–4892

Evans MN, Fairbanks RG, Rubenstone JL (1998) A proxy index of ENSO teleconnections. Nature 394:732–733

Guilderson TP, Schrag DP, Kashgarian M, Southon J (1998) Radiocarbon variability in the western equatorial Pacific inferred from a high-resolution coral record from Nauru Island. J Geophy Res 103:24641–24650

Held IM, Soden BJ (2006) Robust responses of the hydrological cycle to global warming. J Clim 19:5686–5699

Karnauskas KB, Seager R, Kaplan A, Kushnir Y, Cane MA (2009) Observed strengthening of the zonal sea surface temperature gradient across the equatorial Pacific Ocean. J Clim 22:4316–4321

Knutson TR, Manabe S (1995) Time-mean response over the tropical Pacific to increased CO_2 in a coupled ocean-atmosphere model. J Clim 8:2181–2199

Lindzen RS, Nigam S (1987) On the role of sea surface temperature gradients in forcing low-level winds and convergence in the tropics. J Atmos Sci 44:2418–2436

Linsley BK, Dunbar RB, Wellington GM, Mucciarone DA (1994) A coral-based reconstruction of intertropical convergence zone variability over Central America since 1707. J Geophys Res 99(C5):9977–9994

Linsley BK, Ren L, Dunbar RB, Howe SS (2000) El Nino Southern Oscillation (ENSO) and decadal-scale climate variability at 10 N

in the eastern Pacific from 1893 to 1994: a coral-based reconstruction from Clipperton Atoll. Paleoceanography 15(3): 322–335

Quinn TM, Taylor FW, Crowley TJ (2006) Coral-based climate variability in the Western Pacific Warm Pool since 1867. J Geophys Res 111:C11006. doi:10.1029/2005JC003243

Rayner NA, Parker DE, Horton EB, Folland CK, Alexander LV, Rowell DP, Kent EC, Kaplan A (2003) Global analyses of sea surface temperature, sea ice, and night marine air temperature since the late nineteenth century. J Geophys Res 108:4407. doi: 10.1029/2002JD002670

Reynolds RW, Smith TM, Liu C, Chelton DB, Casey KS, Schlax MG (2007) Daily high-resolution blended analyses for sea surface temperature. J Climate 20:5473–5496

Seager R, Murtugudde R (1997) Ocean dynamics, thermoclime adjustment, and regulation of tropical SST. J Clim 10:521–534

Shen GT, Cole JE, Lea DW, Linn LJ, McConnaughey TA, Fairbanks RG (1992) Surface ocean variability at Galapagos from 1936–1982: calibration of geochemical tracers in corals. Paleoceanography 7:563–588

Sugi M, Noda A, Sato N (2002) Influence of the global warming on tropical cyclone climatology: an experiment with the JMA global model. J Meteorol Soc Jpn 80:249–272

Sun D-Z, Liu Z (1996) Dynamic ocean-atmosphere coupling: a thermostat for the tropics. Science 272:1148–1150

Tudhope AW, Shimmield GB, Chilcott CP, Jebb M, Fallick AE, Dalgleish AN (1995) Recent changes in climate in the far western equatorial Pacific and their relationship to the Southern Oscillation; oxygen isotope records from massive corals, Papua New Guinea. Earth Planet Sci Lett 136:575–590

Urban FE, Cole JE, Overpeck JT (2000) Influence of mean climate change on climate variability from a 155-year tropical Pacific coral record. Nature 407:989–993

Vecchi GA, Soden BJ (2007) Global warming and the weakening of the tropical circulation. J Clim 20:4316–4340

Vecchi GA, Soden BJ, Wittenberg AT, Held IM, Leetmaa A, Harrison MJ (2006) Weakening of tropical Pacific atmosphere circulation due to anthropogenic forcing. Nature 441:73–76

Walker GT (1924) Correlation in seasonal variations of weather. IX. A further study of world weather. Mem Indian Meteorol Dep 24(Part 9):275–332

Xie S-P, Deser C, Vecchi GA, Ma J, Teng H, Wittenberg AT (2010) Global warming pattern formation: sea surface temperature and rainfall. J Clim 23:966–986